Available online at www.sciencedirect.com
ScienceDirect
Journal of Power Sources 162 (2006) 502–512
JOURNAL OF POWER SOURCES
www.elsevier.com/locate/jpowsour

Rapid self-start of polymer electrolyte fuel cell stacks from subfreezing temperatures

R.K. Ahluwalia*, X. Wang

Nuclear Engineering Division, Argonne National Laboratory, Argonne, IL 60439, United States

Received 24 May 2006; received in revised form 25 June 2006; accepted 26 June 2006
Available online 9 August 2006

Abstract

Polymer electrolyte fuel cell (PEFC) systems for light-duty vehicles must be able to start unassisted and rapidly from temperatures below −20 °C. Managing buildup of ice within the porous cathode catalyst and electrode structure is the key to self-starting a PEFC stack from subfreezing temperatures. The stack temperature must be raised above the melting point of ice before the ice completely covers the cathode catalyst and shuts down the electrochemical reaction. For rapid and robust self-start it is desirable to operate the stack near the short-circuit conditions. This mode of operation maximizes hydrogen utilization, favors production of waste heat that is absorbed by the stack, and delays complete loss of effective electrochemical surface area by causing a large fraction of the ice to form in the gas diffusion layer rather than in the cathode catalyst layer. Preheating the feed gases, using the power generated to electrically heat the stack, and operating pressures have only small effect on the ability to self-start or the startup time. In subfreezing weather, the stack shut-down protocol should include flowing ambient air through the hot cathode passages to vaporize liquid water remaining in the cathode catalyst. Self-start is faster and more robust if the bipolar plates are made from metal rather than graphite.

Keywords: Polymer electrolyte fuel cells; Startup from subfreezing temperatures; Automotive propulsion systems

1. Introduction

To be competitive with the internal combustion engines, fuel cells for light-duty vehicles must be able to start unassisted from temperatures below −20 °C and produce 90% of rated power within a short time, preferably less than 30 s [1]. A problem with startup from subfreezing temperatures is that the water produced at the cathode from the electrochemical reaction turns into ice and coats the catalyst. The portion of the catalyst surface that is covered with ice is not available to conduct the reaction. Thus, a stage may be reached where the cathode catalyst is completely engulfed in ice and the electrochemical reaction shuts down.

It may be feasible to avoid ice formation at startup by running the fuel cell under conditions at which air does not become saturated. At subfreezing temperatures, however, air has a limited capacity to hold water vapor since the vapor pressure of water is only 0.0028 bar at −10 °C and 0.0012 bar at −20 °C. Thus, the cell must be operated at a very high cathode stoichiometry, defined as the ratio of air flow rate to the theoretical amount needed for complete oxidation of hydrogen. High stoichiometry can be achieved by operating the cell at low currents or at high flow rates. The maximum flow rate is always limited by the capacity of the air management system (i.e., blower in an ambient-pressure system or a compressor in a pressurized system). Furthermore, maintaining a high flow rate causes a large amount of heat to be convected out and slows the process of heating the cell. Operating the cell at low currents is also counterproductive in that the corresponding hydrogen conversion is small as is the heat generated from the electrochemical reaction. Thus, the stack heats up slowly if it is operated at a low current density.

The purpose of this study is to investigate operating conditions under which a PEFC stack can be self-started from subfreezing temperatures. The study has been conducted by developing a simple model that is capable of tracking the formation and melting of ice within the porous catalyst and electrode structures. The model is validated by analyzing voltage decay

* Corresponding author.
E-mail address: walia@ne.anl.gov (R.K. Ahluwalia).

0378-7753/$ – see front matter © 2006 Elsevier B.V. All rights reserved.
doi:10.1016/j.jpowsour.2006.06.071

Nomenclature

a	activity
A	membrane area
c_p	specific heat
D	diffusivity
E	potential
f	volume fraction
F	Faraday constant
h	enthalpy
I	current density
I_0	exchange current density
k	mass transfer coefficient
L	catalyst loading
m	mass
$\dot{m}$	mass flow rate
M	molecular weight
N	molar flow rate
P	pressure
R	gas constant
t	time
T	temperature
X	mole fraction
z	transverse direction

Greek symbols

α	coefficient of net water transport across membrane
δ	thickness
η	overpotential
λ	water content of membrane
ρ	density
σ	conductivity
τ	tortuosity

Subscripts/superscripts

a	anode
ae	anode electrode
c	cathode
ce	cathode electrode
e	electronic
g	gas
i	ionic, ice
l	liquid water
p	bipolar plate
s	cell structure, saturation
w	water

data from single-cell experiments conducted under isothermal conditions. The validated model is then used in a parametric study on non-isothermal start of an automotive stack from sub-freezing temperatures. Some parameters included in the study are cell voltage, initial temperature, materials of construction, operating pressure, oxidant flow rate and the stack shut-down protocol.

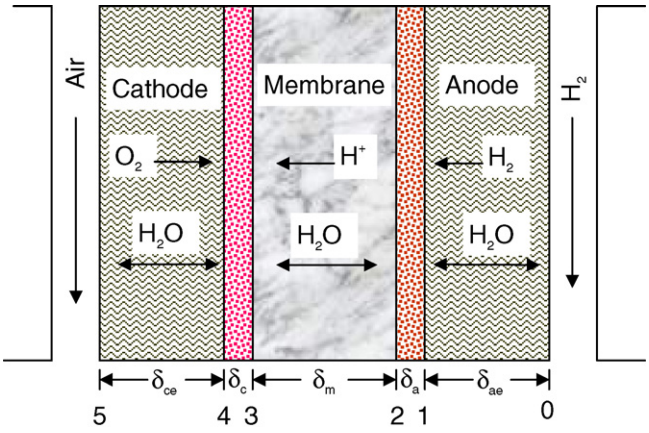

Fig. 1. Nomenclature used in model formulation.

2. Model formulation

A detailed 2D model was developed to determine the electric field, current distribution, species concentrations and formation and melting of ice within a representative cell [2]. It constitutes the basis for formulating a simpler model that captures the essential results and is more suitable for conducting a parametric study. In the simpler model, the cell voltage V is determined from the Nernst potential E_N and the overpotentials η as

$$V = E_N - \eta_e^{ae} - \eta_g^{ae} - \eta_e^a - \eta_i^a - \eta_g^a - \eta_s^a - \eta_i^m - \eta_e^c - \eta_i^c - \eta_g^c + \eta_s^c - \eta_e^{ce} - \eta_g^{ce} - \eta_e^p \quad (1)$$

In Eq. (1), the subscripts e, i, g and s denote the electronic, ionic, gas phase and activation components of the overpotentials, and the superscripts ae, a, m, c, ce and p represent the anode electrode, anode catalyst, membrane, cathode catalyst, cathode electrode, and the bipolar plate, respectively. With reference to Fig. 1, the various terms in Eq. (1) can be calculated from the following equations:

$$E_N = E_0 + \frac{RT}{2F}\ln(P_{H_2}^{(0)}) + \frac{RT}{4F}\ln(P_{O_2}^{(5)}) - \frac{RT}{2F}\ln(P_w^{(5)}),$$

$$\eta_e^{ae} = \frac{I}{\sigma_e^{ae}}\delta_{ae}, \qquad \eta_g^{ae} = \frac{RT}{2F}\ln\left(\frac{X_{H_2}^{(0)}}{X_{H_2}^{(1)}}\right), \qquad \eta_e^a = \frac{1}{2}\frac{I}{\sigma_e^a}\delta_a,$$

$$\eta_i^a = \frac{1}{2}\frac{I}{\sigma_i^a}\delta_a, \qquad \eta_g^a = \frac{RT}{2F}\ln\left(\frac{X_{H_2}^{(1)}}{X_{H_2}^{(2)}}\right), \qquad \eta_i^m = \frac{I}{\sigma_i^m}\delta_m,$$

$$\eta_e^c = \frac{1}{2}\frac{I}{\sigma_e^c}\delta_c, \qquad \eta_i^c = \frac{1}{2}\frac{I}{\sigma_i^c}\delta_c,$$

$$\eta_g^c = \frac{RT}{4F}\ln\left(\left(\frac{X_{O_2}^{(4)}}{X_{O_2}^{(3)}}\right)\left(\frac{X_w^{(3)}}{X_w^{(4)}}\right)^2\right), \qquad \eta_e^{ce} = \frac{I}{\sigma_e^{ce}}\delta_{ce},$$

$$\eta_g^{ce} = \frac{RT}{4F}\ln\left(\left(\frac{X_{O_2}^{(5)}}{X_{O_2}^{(4)}}\right)\left(\frac{X_w^{(4)}}{X_w^{(5)}}\right)^2\right), \qquad \eta_e^p = \frac{I}{\sigma_e^p}\delta_p \quad (2)$$

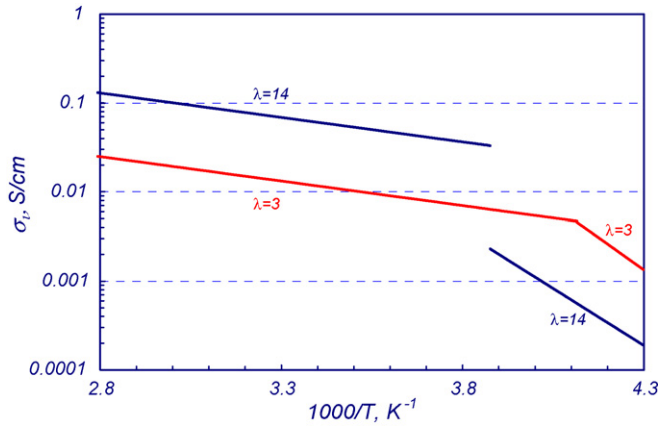

Fig. 2. Correlation for Nafion conductivity as a function of temperature and water content.

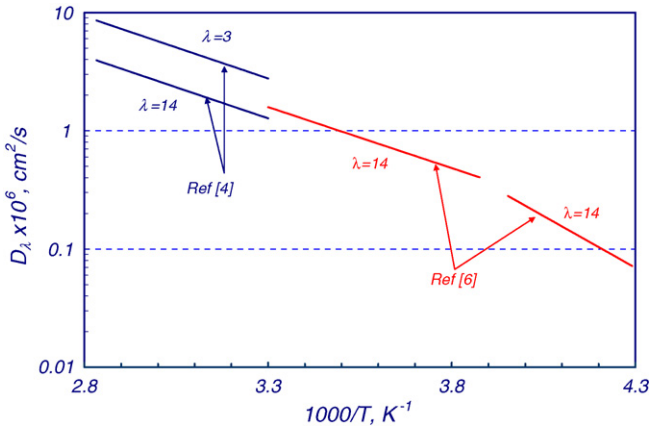

Fig. 3. Correlation for water diffusivity in Nafion as a function of temperature and water content.

Following Ref. [3], the ionic conductivity of the porous anode and cathode catalysts may be estimated from their ionomer contents as

$$\sigma_{\mathrm{i}}^{\mathrm{a}} = \sigma_{\mathrm{i}}\left[(1-\varepsilon_{\mathrm{a}})f_{\mathrm{m}}^{\mathrm{a}}\right]^{1.5}, \quad \sigma_{\mathrm{i}}^{\mathrm{c}} = \sigma_{\mathrm{i}}[(1-\varepsilon_{\mathrm{c}})f_{\mathrm{m}}^{\mathrm{c}}]^{1.5} \tag{3}$$

The electronic conductivity of the porous catalysts similarly may be estimated from their carbon contents. Also, the average ionic conductivity of the membrane $\sigma_{\mathrm{l}}^{\mathrm{m}}$ is given by the following integral:

$$\frac{1}{\sigma_{\mathrm{i}}^{\mathrm{m}}} = \frac{1}{\delta_{\mathrm{m}}}\int \frac{\mathrm{d}z}{\sigma_{\mathrm{i}}} \tag{4}$$

In order to calculate $\sigma_{\mathrm{i}}^{\mathrm{m}}$ from Eq. (4) we need to determine the λ profile in the membrane by considering water transport by diffusion and electro-osmotic drag [4]:

$$-\frac{\rho_{\mathrm{m}}}{M_{\mathrm{m}}}D_\lambda\frac{\mathrm{d}\lambda}{\mathrm{d}z} + \frac{2.5\lambda}{22}\frac{I}{F} = \frac{\alpha I}{F} \tag{6}$$

Fig. 3 shows our approach for integrating the D_λ correlation given in Ref. [4] for the 30–80 °C operating temperature range with the low-temperature data (−130 to 30 °C) reported in Ref. [6]. The combined correlation given below has discontinuity in D_λ ($\mathrm{cm^2\,s^{-1}}$) with steeper temperature dependence below −15 °C:

$$D_\lambda = \frac{1}{(1+0.0126\lambda)^2}\frac{\lambda}{(17.81-77.9a+108a^2)}D_{\mathrm{w}}, \qquad \lambda = 0.043+17.81a-39.85a^2+36a^3,$$

$$D_{\mathrm{w}} = \begin{cases} (-0.026\lambda^2+0.81\lambda-0.73)\times 10^{-6}\exp\left[2416\left(\dfrac{1}{303}-\dfrac{1}{T}\right)\right] & T > -15\,^\circ\mathrm{C} \\ 3.2\times 10^{-6}\exp\left[4030\left(\dfrac{1}{233}-\dfrac{1}{T}\right)\right] & T < -15\,^\circ\mathrm{C} \end{cases} \tag{7}$$

Fig. 2 shows our approach for integrating the Nafion conductivity correlation given in Ref. [4] for the 30–80 °C operating temperature range with the low-temperature data (−130 to 20 °C) reported in Ref. [5]. A λ-dependent activation energy was derived from the low-temperature data by assigning a λ of 3 to the type B membrane stored in air (5% H_2O by mass) and a λ of 14 to the type C membrane stored in water (20–25% H_2O by mass). In combining the two sets of data, it was assumed that there is a jump discontinuity in σ_{i} at −15 °C for λ = 14 but σ_{i} is continuous for λ < 3. Between λ of 3 and 14, the jump temperature, which may be indicative of freezing of excess water in the membrane, is taken as a function of λ. We propose the following hybrid correlation for σ_{i} ($\mathrm{S\,m^{-1}}$) as a function of temperature and water content (λ):

$$\sigma_{\mathrm{i}}(\lambda,T) = \begin{cases} (0.5139\lambda-0.326)\exp\left[1268\left(\dfrac{1}{303}-\dfrac{1}{T}\right)\right] & T > (238.9+1.36\lambda) \\ 1.6\times 10^{-8}\exp\left[(6890-45.3\lambda)\left(\dfrac{1}{150}-\dfrac{1}{T}\right)\right] & T \le (238.9+1.36\lambda) \end{cases} \tag{5}$$

We have used the Butler–Volmer equation for estimating the activation overpotentials for the hydrogen oxidation reaction on the anode and oxygen reduction reaction on the cathode [7]:

$$I = I_0^{\mathrm{a}}L_{\mathrm{Pt}}^{\mathrm{a}}A_{\mathrm{Pt}}^{\mathrm{a}}\left[\exp\left(\frac{2\eta_{\mathrm{s}}^{\mathrm{a}}F}{RT}\right)-\exp\left(\frac{-2\eta_{\mathrm{s}}^{\mathrm{a}}F}{RT}\right)\right],$$

$$I + I^x = I_0^{\mathrm{c}}L_{\mathrm{Pt}}^{\mathrm{c}}A_{\mathrm{Pt}}^{\mathrm{c}}\left[\exp\left(\frac{\eta_{\mathrm{s}}^{\mathrm{c}}F}{RT}\right)-\exp\left(\frac{-\eta_{\mathrm{s}}^{\mathrm{c}}F}{RT}\right)\right] \tag{8}$$

The cross-over current density I^x may be related to the H_2 permeation flux as follows:

$$\frac{I^x}{2F} = \frac{\psi_{\mathrm{H_2}}}{\delta_{\mathrm{m}}}P_{\mathrm{H_2}}^{\mathrm{a}} \tag{9}$$

Ref. [7] may be consulted for the dependence of exchange current densities on temperature and partial pressures of H_2 and O_2. We assume a linear relationship between the effective electrochemical surface area (ECSA) of the Pt catalyst and the volume fractions of water and ice in the cathode layer:

$$A^{c}_{Pt} = A^{0}_{Pt}(1 - f^{c}_{i} - f^{c}_{l}) \tag{10}$$

Finally, we solve the Stefan–Maxwell equations to calculate the profiles of H_2, O_2 and H_2O concentrations across the porous catalysts and electrodes:

$$\frac{dX_i}{dz} = \frac{RT}{P}\sum \frac{X_i N_j - X_j N_i}{D^{e}_{ij}},$$

$$D^{e}_{ij} = \frac{D_{ij}\left[\varepsilon(1 - f_i - f_l)\right]^{1.5}}{\tau} \tag{11}$$

2.1. Flow and heat transfer model

In the anode gas channel, the following equations describe the changes in molar flow rates of H_2 and water vapor due to H_2 oxidation, H_2 permeation, O_2 permeation, and water transport through the membrane. It is assumed that O_2 that permeates from the cathode side instantaneously reacts with H_2 to form water:

$$\frac{dN_{H_2}}{dA} = -\frac{I}{2F} - \frac{\psi_{H_2}}{\delta_m}P^{a}_{H_2} - \frac{2\psi_{O_2}}{\delta_m}P^{c}_{O_2},$$

$$\frac{dN_w}{dA} = -\frac{\alpha I}{F} + \frac{2\psi_{O_2}}{\delta_m}P^{c}_{O_2} \tag{12}$$

Similar equations have been written for molar flow rates of O_2 and water vapor in the cathode gas channel. Below 0 °C, it is assumed that the source term for H_2O is determined by the transport of water vapor through the porous catalyst and electrode and across the gas channel. As above, it is assumed that H_2 that permeates from the anode side instantaneously reacts with O_2 to form water:

$$\frac{dN_{O_2}}{dA} = -\frac{I}{4F} - \frac{\psi_{O_2}}{\delta_m}P^{c}_{O_2} - \frac{\psi_{H_2}}{2\delta_m}P^{a}_{H_2},$$

$$\frac{dN_w}{dA} = \begin{cases} k_w(\rho^{(4)}_w - \rho^{(5)}_w) & T \le 0\,^{\circ}C \\ \dfrac{(1+2\alpha)I}{2F} + \dfrac{\psi_{H_2}}{\delta_m}P^{a}_{H_2} & T > 0\,^{\circ}C \end{cases} \tag{13}$$

Below 0 °C, the fraction of water that turns into ice can be determined from the current density and the rates of transport of water across the membrane, H_2 permeation and transport of water vapor to the gas channel. Let f_D be the fraction of ice that is formed in the cathode catalyst layer (CCL) and $(1 - f_D)$ the fraction that is formed in the cathode gas diffusion layer (GDL). Then we can track the accumulation of ice in the porous cathode and electrode by solving the following equations:

$$\varepsilon_c\delta_c\rho_i\frac{df^{c}_{i}}{dt} = f_D\left[\frac{(1+2\alpha)I}{2F} + \frac{\psi_{H_2}}{\delta_m}P^{a}_{H_2} - k_w(\rho^{(4)}_w - \rho^{(5)}_w)\right],$$

$$\varepsilon_{ce}\delta_{ce}\rho_i\frac{df^{ce}_{i}}{dt} = (1 - f_D) \times \left[\frac{(1+2\alpha)I}{2F} + \frac{\psi_{H_2}}{\delta_m}P^{a}_{H_2} - k_w(\rho^{(4)}_w - \rho^{(5)}_w)\right] \tag{14}$$

Above 0 °C, liquid water forms in the cathode catalyst layer and the GDL. For brevity and because details are available elsewhere [8], we have omitted the formulation used for determining the liquid saturation profiles in the porous structures. Also, see Ref. [9] for the permeation coefficients ψ_{H_2} and ψ_{O_2}.

Under certain conditions ice may also form within the porous anode catalyst and electrode. For those cases, it is quite straightforward to derive an equation similar to Eq. (14) in order to track ice accumulation within the anode structure.

Finally, the temperature profile is determined by solving the following equation:

$$\frac{\partial}{\partial t}(m_s h_s + m_w h_w) + \frac{\partial}{\partial A}(\dot{m}_c h_c + \dot{m}_a h_a) = -\left[\frac{(1+2\alpha)I}{2F} + \frac{\psi_{H_2}}{\delta_m}P^{a}_{H_2} - k_w(\rho^{(4)}_w - \rho^{(4)}_w)\right]h_w - VI \tag{15}$$

where m_s and m_w are the mass of structure and condensate per unit membrane area, and the enthalpy of condensate h_w is given as follows:

$$h_w = \begin{cases} h^{0}_{i} + c_{pi}T & T \le 0\,^{\circ}C \\ h^{0}_{l} + c_{pl}T & T > 0\,^{\circ}C \end{cases} \tag{16}$$

2.2. Method of solution

An implicit finite-difference scheme was used to solve Eqs. (1)–(15). The cell was divided into 5–50 nodes. Eqs. (14) and (15) were discretized in time and space and Eqs. (12) and (13) were discretized in space. At each time step, a marching algorithm was used to solve the resulting non-linear algebraic equations from cell inlet to outlet. At each axial node, Eq. (6) was numerically solved for transverse profile of λ across the membrane and Eq. (11) for species distribution across the cathode and anode catalysts and electrodes.

3. Model validation with isothermal data

Hishinuma et al. [10] assembled a 104-cm^2 cell and investigated its startup behavior from −10 to −25 °C at 1–2 bar. The cell membrane electrode assembly (MEA) was formed from a 30-μm Gore-Tex membrane coated with 16-μm thick catalyst layers that have 1.4×10^4 cm^2 cm^{-3} initial electrochemical surface area. Graphite fiber cloths, 470 μm in thickness and 40% porosity, served as gas diffusion layers. Graphite plates with ribbed channels were used to distribute gases. The assembled single-cell apparatus was positioned inside an environmental control chamber to maintain a constant temperature over the

Table 1
Critical current density above which ice is formed

T (°C)	P (atm)	Flow rate (L min^{-1})		I_c (mA cm^{-2})		
		Air	H_2	Test	Eq. (17)	Eq. (18)
−25	1	2.83	0.66	<1	2.9 ($\alpha = -0.17$)	2.0 ($\alpha = -0.17$)
−20	1	9.49	1.19	3	14.5 ($\alpha = -0.1$)	5.1 ($\alpha = -0.15$)
−10	1	6.33	0.79	10	23.5 ($\alpha = -0.1$)	9.2 ($\alpha = -0.16$)
−10	1.5	6.33	0.79		15.6 ($\alpha = -0.1$)	6.3 ($\alpha = -0.14$)
−10	2	6.33	0.79		11.75 ($\alpha = -0.1$)	4.7 ($\alpha = -0.12$)

duration of a test. Dry bottled gases were used to supply hydrogen as fuel and a 79% N_2–21% O_2 synthetic mixture as oxidizer. The tests monitored voltage decay at constant current.

3.1. Critical current density

The tests (conducted under isothermal conditions) measured the critical current density (I_c) above which the cell voltage steadily declined with time and below which the cell could operate stably. Arguably ice is formed within the MEA only if the current density exceeds I_c. We associate I_c with two limiting conditions, the less stringent of which is that ice is formed if the water produced by the electrochemical reaction is sufficient to saturate the cathode stream. With this criterion and accounting for water transferred between the anode and cathode streams, I_c may be calculated from the following equation:

$$\frac{I_c}{2F} = \frac{X_{ws}}{1 + (1 - X_{ws})(1 + 4\alpha)} \left(\frac{N_{air}}{A} \right) \tag{17}$$

Table 1 compares the experimentally measured critical current density with I_c calculated from Eq. (17). The comparison shows that Eq. (17) overestimates the critical current density and suggests that the gas phase need not be saturated for ice to form. We therefore postulate a more stringent condition that ice is formed if the flux of water produced from the electrochemical reaction locally exceeds the rate at which it can diffuse from the porous catalyst to the cathode gas channel. According to this criterion, I_c may be calculated from the following equation:

$$\frac{I_c}{2F} = \frac{k_w(\rho_{ws} - \rho_w)}{(1 + 2\alpha)} \tag{18}$$

Table 1 shows that I_c calculated from Eq. (18) agrees reasonably well with the experimentally measured critical current densities. It is worth mentioning that calculating average I_c is somewhat involved since the local vapor density (ρ_w) is unknown and Eq. (18) calculates the local rather than the average current density. We calculate ρ_w by integrating an equation for water vapor density from the inlet to the outlet of the cathode gas channel. We then iteratively determine the average I_c such that Eq. (18) is satisfied at the cathode outlet where ice is formed first.

3.2. Transport function

Water produced from the electrochemical reaction either diffuses to the gas channel and is convected out or condenses within the MEA. At subfreezing conditions, a fraction of the condensate appears as ice in the cathode catalyst layer and the remaining as ice in the gas diffusion layer. The fraction that appears as ice in the GDL (f_D) depends on the water production rate (i.e., current density), the rate at which water vapor diffuses from the CCL to the GDL, and vapor condensation kinetics. Although it is possible to calculate f_D theoretically, it is simpler to infer it from the experimental data itself. We infer f_D from the observed time for the cell voltage to decline to zero (t_s) at constant current density (I). We assume that only I in excess of I_c contributes to formation of ice and that at $t = t_s$ the CCL is completely engulfed in ice. With these assumptions f_D can be estimated from the following equation:

$$f_D = 1 - \frac{\varepsilon_c \delta_c \rho_i / M_w}{t_s(I - I_c)/2F} \tag{19}$$

Fig. 4 presents the inferred f_D as a function of current density at different temperatures and pressures. It indicates that as the current density is increased a larger fraction of water appears as ice in the GDL. It also suggests that f_D decreases with pressure but is only a weak function of temperature.

For use in our model, f_D was curve-fitted in terms of two product functions, one that depends only on the current density (A cm^{-2}) and the other on pressure (bar) as follows:

$$f_D = 0.85[1 - \exp(-74I)][0.85 + 0.15\exp(-1.67(P - 1))] \tag{20}$$

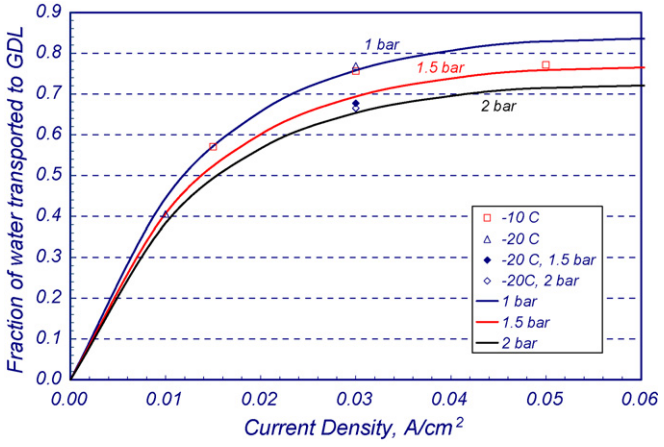

Fig. 4. Empirical correlation for f_D as a function of current density and pressure.

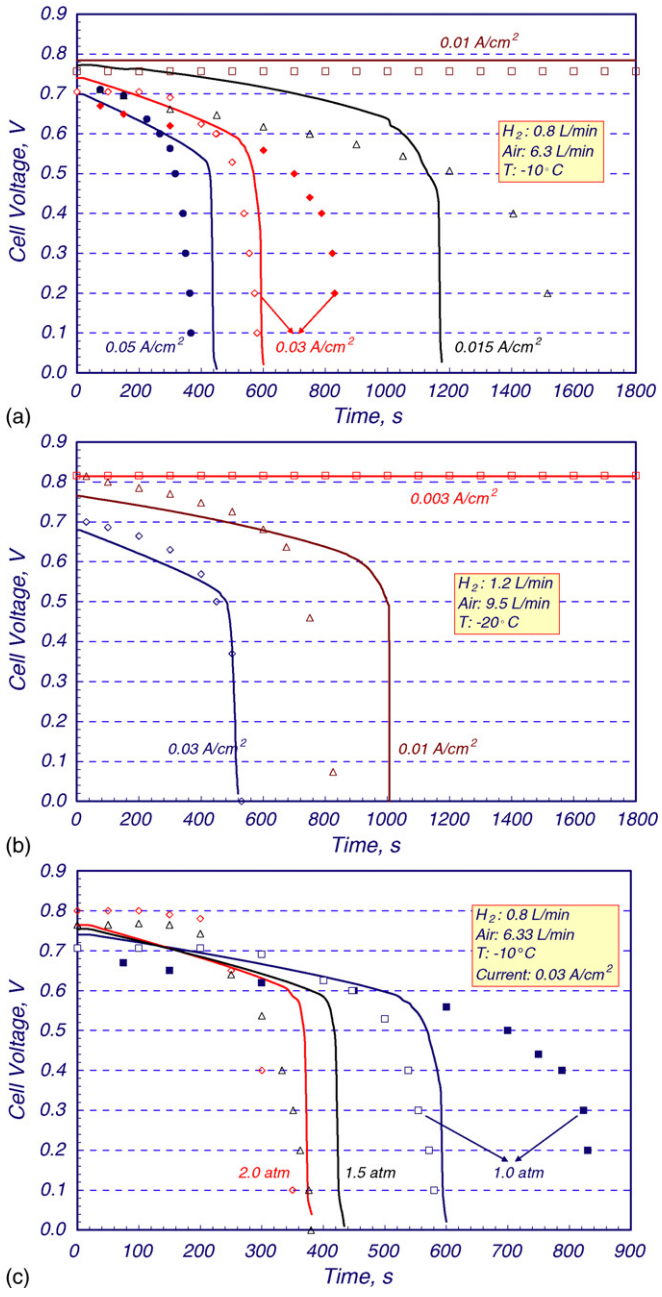

Fig. 5. Measured and calculated isothermal voltage decay profiles: (a) −10 °C, (b) −20 °C, and (c) 1–2 bar at −10 °C.

3.3. Voltage decay profiles

With f_D given by Eq. (20), Fig. 5 shows a favorable comparison between the calculated and observed voltage profiles. At −10 °C and 1 bar, Fig. 5a indicates that the cell voltage is stable at 0.01 A cm^{-2}, declines with time at 0.015 A cm^{-2}, and declines even faster at 0.03–0.05 A cm^{-2}. At current densities higher than I_c the voltage decline is gradual initially but very rapid once the ice volume fraction in the CCL exceeds 0.8–0.9 in our model. The cell voltage becomes less than 0.1 V at 1200 s (1460 s in the test) at 0.015 A cm^{-2}, 600 s (600–820 s in the test) at 0.03 A cm^{-2}, and 420 s (380 s in the test) at 0.05 A cm^{-2}. The data from the two different tests at 0.03 A cm^{-2} are not entirely reproducible presumably because of incomplete removal of ice from the MEA resulting in different initial conditions [11]. Between the tests, the ice deposited in the MEA was removed by flowing dry gases without passing current.

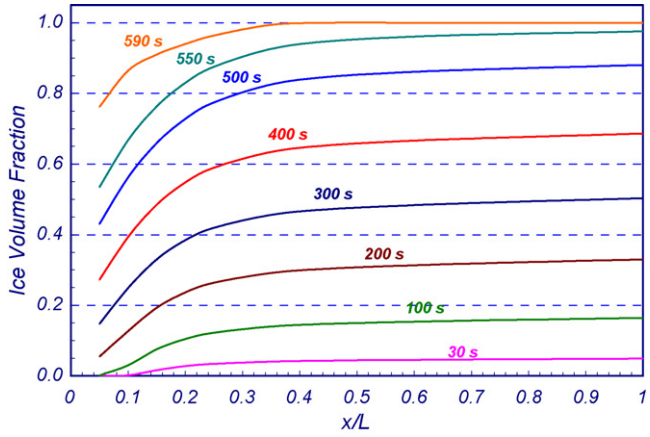

Fig. 6. Progressive formation of ice at −10 °C, P = 1 bar, I = 0.03 A cm^{-2}.

Fig. 5b compares the calculated and measured voltage decay profiles at −20 °C and 1 bar. Compared to the results in Fig. 5a for −10 °C, I_c is smaller as is the initial cell voltage at the same I and the voltage decays at a faster rate. For example, at 0.03 A cm^{-2}, the cell voltage becomes less than 0.1 V at about 520 s at −20 °C compared to 600 s at −10 °C.

Fig. 5c presents the calculated and measured effect of pressure on voltage profiles at −10 °C and 0.03 A cm^{-2}. Both the model and experimental data indicate faster decline in cell voltage at higher pressure. In our model, the operating pressure affects both the critical current density I_c (see Table 1) and the transport function f_D. The higher the operating pressure the smaller the critical current density and the fraction of condensate that forms in the GDL, so that ice builds up more rapidly in the CCL.

Fig. 6 presents the modeled profiles of ice volume fraction in CCL at different times at −10 °C, 1 bar and 0.03 A cm^{-2}. As mentioned earlier, ice begins to form at the channel exit if the average current density equals I_c. For the operating conditions of Fig. 6, $I > I_c$, so that ice begins to form at an upstream location. The portion of the MEA that has CCL covered with ice progressively carries a smaller fraction of the current load. Because the cell is being operated in the constant current mode, the current density has to increase in the upstream portion so that the freeze front advances in time and may reach cathode inlet.

4. Non-isothermal startup from subfreezing temperatures

We have used the model described above to study the startup behavior of a 45-kW PEFC stack from subfreezing temperatures. In combination with a hybrid battery, two of these stacks electrically connected in series can propel a light-duty vehicle [12]. We consider that the MEA for each cell of the stack consists of a 50-μm thick, 1100-EW Nafion membrane coated with a 7-μm thick anode catalyst layer and a 13-μm thick cathode

catalyst layer. The thin-layer anode and cathode are prepared from carbon-supported Pt (47 wt.% Pt/C) in organic ionomer solutions (5 wt.% 1100-EW Nafion) with an ionomer/carbon ratio of 0.8. The Pt loading is 0.4 mg cm^{-2} on cathode and 0.2 mg cm^{-2} on anode. These electrodes have been well characterized in Ref. [7] in terms of porosity (0.4), electrochemical surface area (52 m^2_{Pt}/g_{Pt}), exchange current density and other structural and kinetic parameters. We consider that 275-μm woven carbon cloth is used for the gas diffusion layers and that the flow field channels are fabricated from graphite of 2.3-mm average thickness. The stack consists of 230 cells (9.6 cells per inch) with 430 cm^2 cross-sectional area, 85% of which is active. At rated power, each cell generates 195 W of electric power at 0.65-V cell voltage. The stack weighs 52 kg including 13 kg for the endplates, current collector, insulator, outer wrap and tie bolts. The weight of the stack with the coolant channels filled with ethylene glycol is 55 kg.

4.1. Polarization curves

Fig. 7a presents the modeled steady-state polarization curves for the pressurized stack at different temperatures. A number of assumptions have been made in constructing the polarization curves. The operating pressure is variable and a function of air flow rate: 2.5 bar at rated (100%) flow, 2.0 bar at 75% flow, 1.7 bar at 50% flow, 1.3 bar at 25% flow and 1.1 bar at 10% flow. Air and fuel flow rates at every operating point have been calculated by holding oxygen utilization constant at 50% and fuel utilization constant at 70%. Incoming air and hydrogen streams are humidified to 60% relative humidity at the prevailing stack temperature and pressure. In determining the overpotentials below 0 °C, no allowance has been made for loss in ECSA because of coverage of cathode catalyst with ice. Fig. 7b shows the average combined ohmic voltage drop in the membrane (η_i^m), cathode catalyst layer (η_i^c), and the anode catalyst layer $\eta_i{}^a$ as a function of current density and temperature. It indicates that at a given current density, the decrease in cell voltage with decrease in temperature, as seen in Fig. 7a, is primarily due to the greater ohmic overpotential.

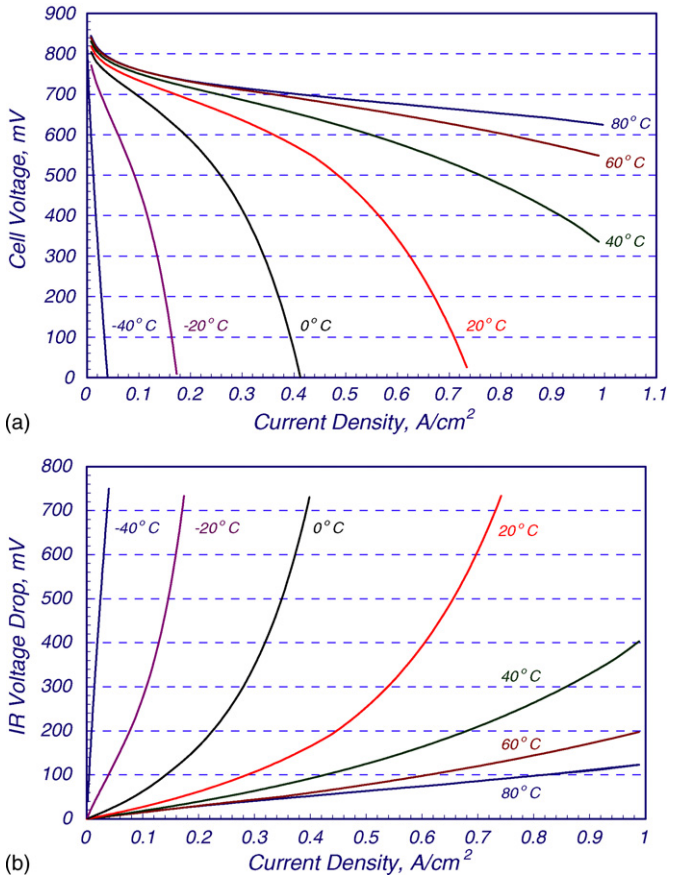

Fig. 7. Modeled steady-state stack behavior at constant anode (2.0) and cathode (1.4) stoichiometries: (a) polarization curves; (b) combined ohmic overpotential in membrane, cathode catalyst layer and anode catalyst layer. The feed gases are humidified at 60% RH and the pressure varies with flow rate.

Fig. 7a shows that the current density at the rated-power point (0.65 V, 80 °C) is 0.82 A cm^{-2}. On the other hand, the short-circuit current densities are calculated as 0.74 A cm^{-2} at 20 °C cell temperature, 0.41 A cm^{-2} at 0 °C, 0.17 A cm^{-2} at −20 °C and 0.04 A cm$_-{}^2$ −40 °C. Thus, as a percent of the hydrogen consumption at rated power, the maximum hydrogen consumption is limited to 90% at 20 °C, 50% at 0 °C, 21% at −20 °C and 5% at −40 °C.

In order to show the effect of ice on the polarization curves at subfreezing temperatures, we present Fig. 8 in which the ice volume fractions in the GDL and CCL are assumed to be equal and the cell temperature is −20 °C. In actual simulations the ice volume fractions in the GDL and CCL are not equal but are determined by solving Eq. (14). Fig. 8 clearly shows that the mass transfer overpotentials become important in our model when the ice volume fraction exceeds 90%. At −20 °C, the short-circuit current is determined by the mass transfer overpotential rather than the ohmic overpotential when $f_i > 0.95$.

4.2. Critical cell voltage for self-start

A number of simulations have been run to analyze the startup of the stack from subfreezing temperatures. Fig. 9 presents the results from one set of simulations in which the stack is initially free of ice at −20 °C, the ambient temperature is also

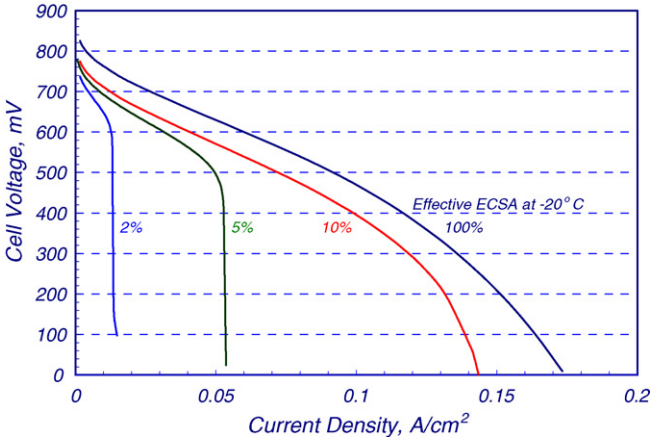

Fig. 8. Effect of ice coverage on polarization curves at −20 °C.

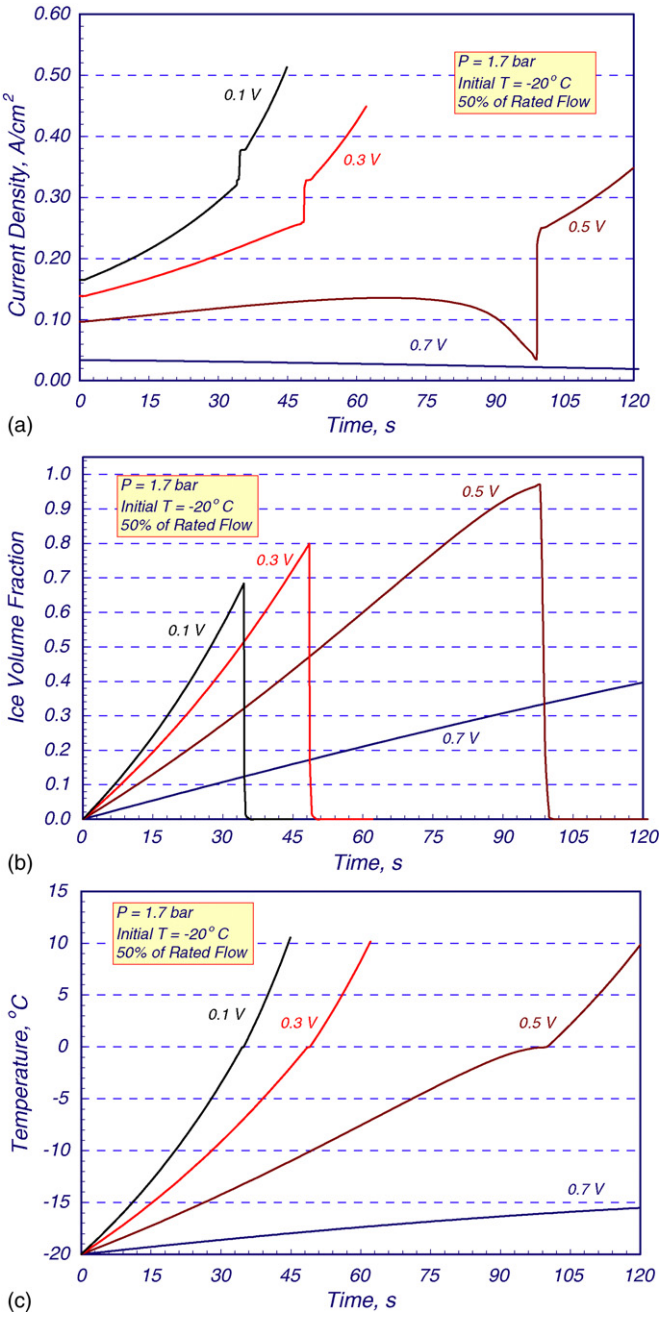

Fig. 9. Effect of cell voltage on startup from −20 °C at constant air and fuel flow rates ($P = 1.7$ bar): (a) current density profiles; (b) ice coverage of cathode catalyst layer; (c) cell temperature.

−20 °C, and the air and hydrogen flows are at 50% of rated capacity.

Unlike the results seen in Fig. 5a and b for isothermal conditions, Fig. 9a points to the existence of a critical cell voltage (V_c) above which self-start is not possible. The critical voltage is a function of the initial stack temperature. The lower the initial stack temperature the lower the critical voltage. At −20 °C, the critical voltage is about 0.5 V. For cell voltage above V_c the average current density decreases monotonically with time (see the curve for 0.7 V) because of the buildup of ice in the cathode catalyst layer. For cell voltage equal to V_c (see the curve for 0.5 V), the current density initially increases with time as the stack heats up but there is an intermediate period of time (75–100 s) during which the current density decreases with time because of diminishing effective ECSA. At 100 s, the ice begins to melt leading to the recovery of ECSA and the current density climbs sharply. For cell voltage below V_c (see the curve for 0.3 V), the startup is faster and more robust in that the current density increases monotonically with time. The startup is even faster if the cell is operated closer to the short-circuit condition, e.g., at 0.1 V rather than at 0.3 V.

Fig. 9b tracks the buildup and disappearance of ice in the cathode catalyst layer. At 0.7 V (i.e., $V > V_c$), ice volume fraction increases gradually. Ice builds up faster if the stack is operated at cell voltage below V_c; however, ice volume fraction reaches a peak value and then decreases precipitously as the stack reaches the ice melting temperature. Below V_c, the lower the cell voltage the smaller the peak value of ice volume fraction.

Fig. 9c presents the stack temperature as a function of time. For $V > V_c$ (0.7 V), the stack is heated slowly and equilibrates at a temperature below the melting point of ice. This is why the stack cannot be self-started from subfreezing temperatures at $V > V_c$. The stack is heated faster and to temperature above the melting point of ice if $V < V_c$. Also, the lower the cell voltage the faster the rise in stack temperature.

There are three reasons why the startup from subfreezing temperatures is faster at near short-circuit conditions ($V \sim 0$, $I \sim I_{sc}$). First, hydrogen utilization is proportional to the amount of current that can be passed. The higher the current the larger the amount of hydrogen consumed in the electrochemical reaction and the faster the rate at which the stack warms up.

Second, the higher the current density the lower the cell voltage and more the waste heat that is generated. At short circuit, the stack does not produce any electrical power. Instead all the heat of reaction is converted into waste heat that is absorbed by the stack.

Third, a fraction of the water that is produced at the cathode is transported into the gas diffusion layer. Fig. 4 indicates that the higher the current density the larger the fraction of water that is transported to GDL. By operating at a high current density we therefore cause a large fraction of ice to form in the GDL rather than in the cathode catalyst layer. This provides additional time to raise the cell temperature above the melting point of ice before the ice can completely cover the cathode catalyst and shut-down the electrochemical reaction.

4.3. Effect of power draw

Startup from subfreezing temperatures can be made faster and more robust if the electric power generated by the stack is used to heat the bipolar plates or the stack coolant. From the standpoint of hardware complexity, it may be easier to electrically heat the coolant rather than the bipolar plates. Fig. 10 indicates that the stack heat up process is accelerated most at 0.5 V—the cell voltage where the power density is highest. The difference is small near the open circuit (0.7 V) and short-circuit (0.1 V) conditions where the stack power density is small.

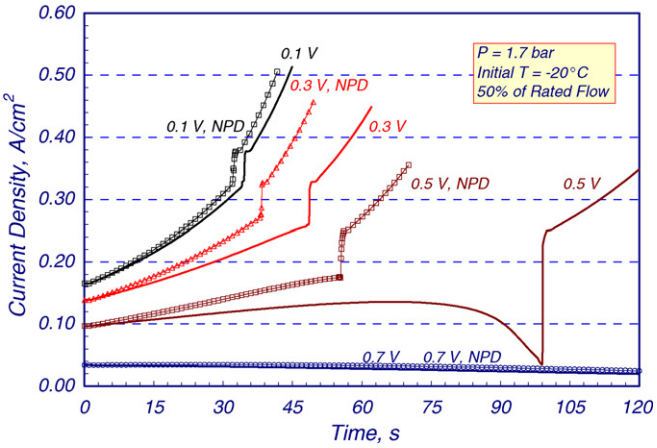

Fig. 10. Effect of power draw on startup from −20 °C.

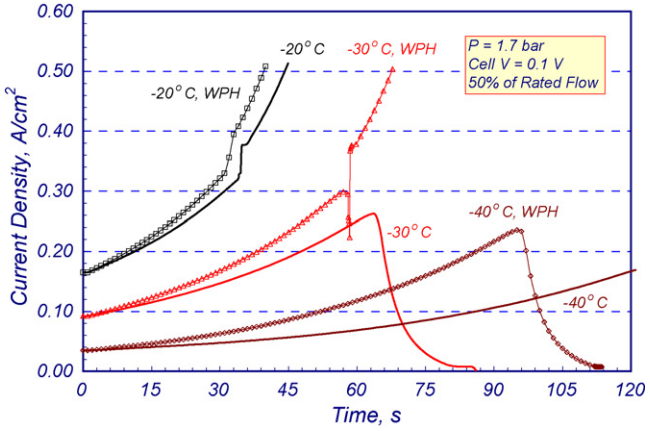

Fig. 12. Effect of preheating feed gases on startup from different temperatures.

4.4. Critical temperature

There is a critical initial temperature (T_c) below which the stack cannot be self-started even at short circuit. Fig. 11 presents the average current density and stack temperature profiles for startup from different initial temperatures at 0.1-V cell voltage. It indicates that the stack temperature can be raised above the melting point of ice if the initial temperature is higher than −20 °C. Self-start is not possible from −40 °C because the cathode catalyst layer is completely coated with ice (terminating the electrochemical reaction) at 130 s when the stack temperature has reached −12 °C only. Similarly, the stack equilibrates at −2 °C for startup from −30 °C initial temperature. External assistance is needed for startup from temperatures below −20 °C.

Fig. 12 illustrates the effect of preheating the feed gases on the critical temperature. Whereas self-start is not possible from −30 °C at 0.1-V cell voltage, the stack temperature can be raised above the melting point of ice by preheating air and hydrogen feeds to 80 °C. Note that even with preheat, the stack cannot be started from −40 °C. Also, preheating feeds is not an effective way of reducing the startup time at temperatures above T_c. For example, preheating feeds to 80 °C reduces the time to heat the stack from −20 to 0 °C by less than 5 s.

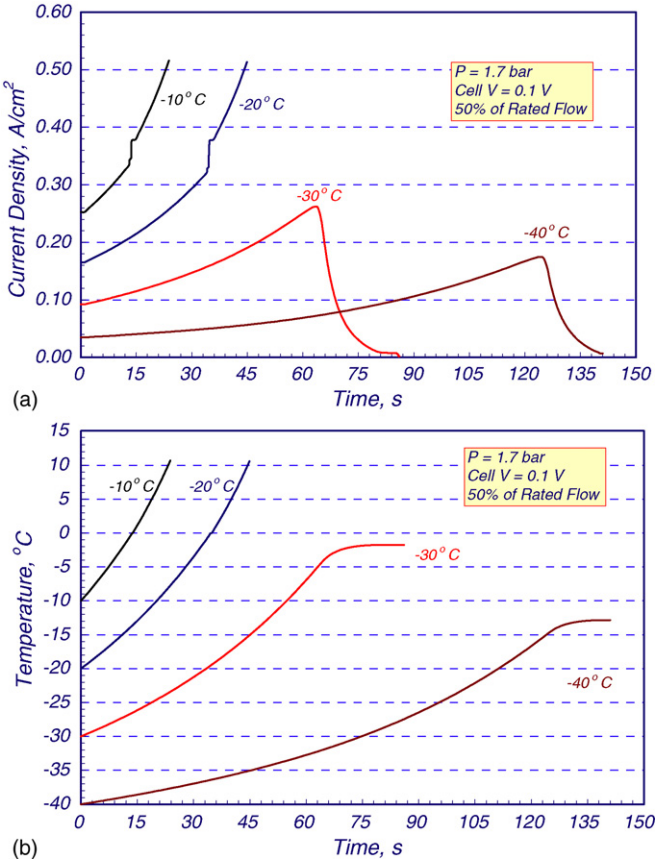

Fig. 11. Effect of initial temperature on startup at 0.1 V: (a) cell current profiles; (b) cell temperature.

4.5. Effect of stack conditioning

Simulations were run to assess the effect of the stack shut-down protocol on subsequent startup from subfreezing temperatures. Fig. 13 presents results from two simulations. In one simulation (DS) the stack is initially dry because the liquid water has been removed from the GDL and the CCL when the stack

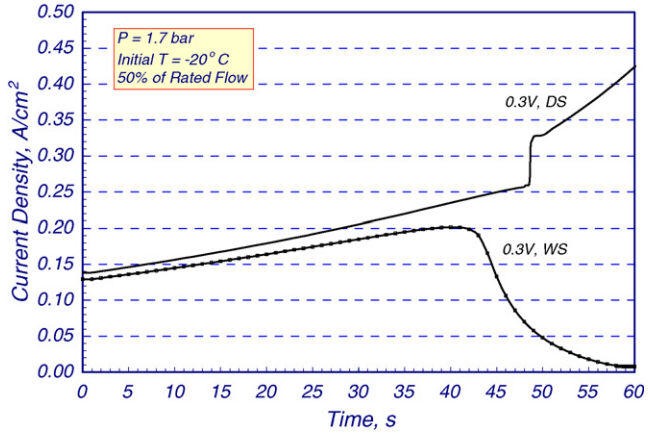

Fig. 13. Effect of shut-down protocol on startup from −20 °C: dry shut-down (DS) vs. wet shut-down (WS).

is shut-down. This can be done, for example, by flowing ambient air over the cathode and vaporizing any remaining liquid water using the thermal energy stored in the bipolar plates. In the second simulation (WS), no specific step is taken to remove the liquid water which subsequently freezes. In the WS simulation, it is assumed that 30% of the pore volume in the GDL and CCL is initially covered with ice. Fig. 13 shows that self-start from −20 °C at 0.3 V is difficult if 30% of ECSA in the cathode catalyst layer is initially unavailable because of ice coverage.

4.6. Metal versus graphite bipolar plates

Although corrosion is a concern, a PEFC stack can be assembled with metal plates that are thinner and lighter than graphite plates. Another advantage of metal plates is that metals have lower specific heat than graphite. For example, the specific heat of stainless steel is 460 J kg^{-1} K compared to 935 J kg^{-1} K for graphite. We ran simulations to investigate the startup behavior of a PEFC stack with 0.43-mm thick stainless steel bipolar plates. Fig. 14 includes results from some simulations that compare the startup of stacks with metal and graphite bipolar plates. It shows that a stack with metal bipolar plates (MP) can be self-started from −40 °C at 0.1 V but a stack with graphite bipolar plates (GP) cannot be self-started at temperatures below −20 °C. Because of smaller thermal inertia, a stack with metal bipolar plates is also quicker to start. For example, it takes less than 20 s to heat a stack with metal bipolar plates from −20 °C to the melting point of ice but almost 35 s if the stack is made with graphite plates.

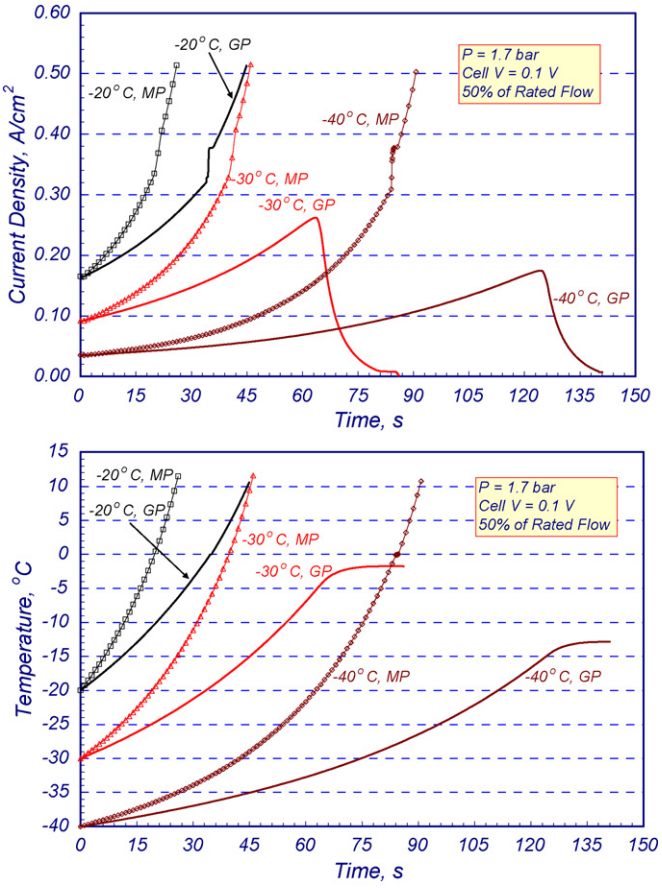

Fig. 14. Effect of bipolar plates on startup at 0.1-V cell voltage: GP and MP denote graphite and metal bipolar plates.

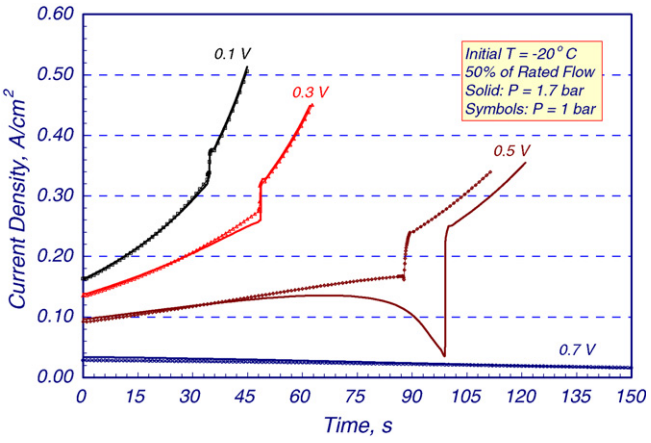

Fig. 15. Effect of operating pressure on startup from −20 °C.

4.7. Ambient-pressure versus pressurized stacks

We ran simulations to analyze the startup behavior of ambient-pressure stacks. Fig. 15 includes results from some simulations that compare the startup of ambient-pressure stacks and pressurized stack (1.7 bar at 50% flow) assuming that the two stacks have the same specific power. It indicates that the ambient-pressure stack is only marginally easier to self-start from −20 °C. Although more water vapor can be convected out with the spent cathode air at 1 bar than at 1.7 bar, the vapor pressure of water at −20 °C is quite low so that a majority of the water formed from the electrochemical reaction turns into ice and is deposited within the MEA.

We also ran simulations to investigate the effect of flow rate on startup of the pressurized stack. Results show only minor differences between startup at 100% (2.5 bar) and at 50% (1.7 bar) of the rated flow. Advantage of the higher flow rate is partially offset by the lower mole fraction of water vapor at saturation so that the fraction of water formed at the cathode that turns into ice is nearly the same at the two flow rates. Also, a larger fraction of the ice formed is retained in the cathode catalyst layer because of the higher pressure at 100% flow with the net result that the startup time is slightly longer at the full flow than at half flow.

4.8. Warm-up time and energy

A number of simulations were run to determine the time and energy needed to heat the pressurized stack to the melting point of ice without external assistance. Fig. 16a summarizes the calculated warm-up time as a function of the cell voltage and the initial temperature. These results are for a stack with graphite bipolar plates. As discussed earlier, the lower the cell voltage the shorter is the warm-up time. Also, for a given initial temperature, there is a critical voltage above which the stack cannot be

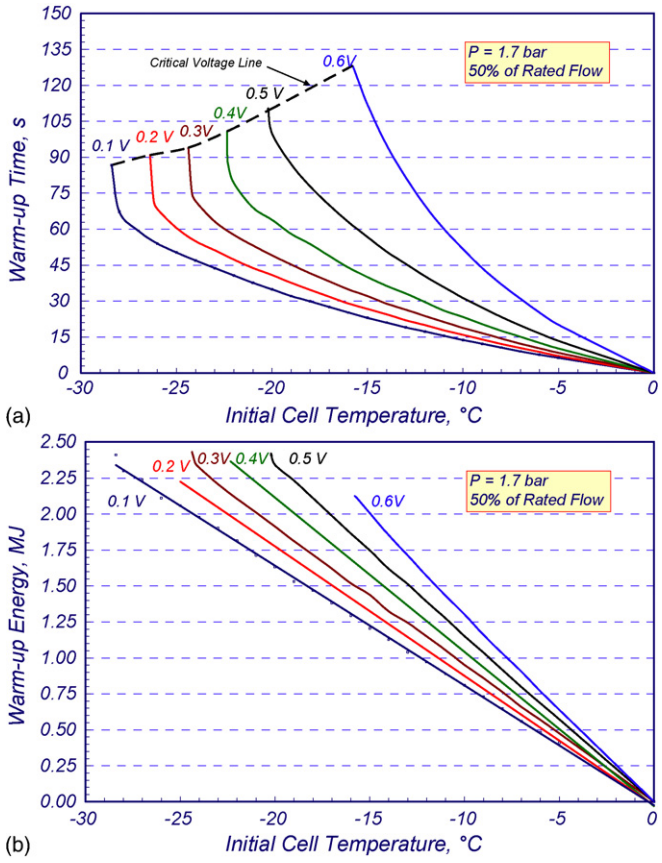

Fig. 16. Effect of initial cell temperature: (a) time to warm-up to 0 °C; (b) warm-up energy.

self-started. If it is desired to minimize the time spent near short circuit, the critical voltage line in Fig. 16a can be followed to raise the cell voltage as the stack warms up.

Fig. 16b presents the corresponding results for the minimum warm-up energy as a function of the cell voltage and the initial temperature. Just as for warm-up time, the lower the cell voltage the smaller is the amount of energy consumed in warming up the stack to 0 °C. Also, the warm-up time and energy can be reduced by using the generated power to electrically heat the stack (or the coolant) or by using metal rather than graphite bipolar plates.

5. Conclusions

Rapid start of a PEFC stack from subfreezing temperatures unavoidably involves formation of ice within the porous cathode catalyst and electrode structure. Managing buildup of ice is the key to obtaining a successful self-start. The stack temperature must be raised above the melting point of ice before the ice completely covers the cathode catalyst and shuts down the electrochemical reaction. Results from our model suggest that for rapid self-start it is desirable to operate the stack near short-circuit conditions. This mode of operation maximizes hydrogen utilization, favors production of waste heat that is absorbed by the stack, and delays complete loss of electrochemical surface area by causing a large fraction of the ice to form in the GDL rather than in the cathode catalyst layer. Other conclusions from this study are highlighted below:

- For a given initial temperature, there exists a critical cell voltage above which self-start is not possible. Conversely, for a given cell voltage, there is a critical temperature below which the stack cannot be self-started.
- Preheating the feed gases to the normal operating temperatures can raise the critical cell voltage but does not significantly reduce the time needed to heat the stack to 0 °C if the stack is operated near short circuit. Using the power generated to electrically heat the bipolar plates or the coolant leads to similar results.
- In subfreezing weather, the stack shut-down protocol should include flowing ambient air through the hot cathode passages to vaporize liquid water remaining in the GDL and the cathode catalyst.
- The coolant in the stack should be isolated from the balance of the coolant in order to minimize the thermal mass that has to be heated during the startup time.
- Because metal plates can be made thinner and generally have lower specific heat, self-start is faster and more robust if the bipolar plates are made from metal rather than graphite.
- Operating pressure has only a small effect on the ability to self-start or the startup time.
- To minimize the time spent near short circuit, the cell voltage can be raised as the stack warms up.

Acknowledgements

This work was supported by the U.S. Department of Energy's Office of Energy Efficiency and Renewable Energy, Office of Hydrogen, Fuel Cells, and Infrastructure Technologies. Dr. Nancy Garland is the program manager at USDOE.

References

[1] Hydrogen, Fuel Cells and Infrastructure Technologies Program: Multi-Year Research, Development and Demonstration Plan, available at: http://www.eere.energy.gov/hydrogenandfuelcells/mypp, 2005.
[2] R.K. Ahluwalia, X. Wang, E.D. Doss, R. Kumar, Fuel cell systems analysis, in: Proceedings of Hydrogen Fuel Cells and Infrastructure Technologies Program Review Meeting, Crystal City, VA, 2005.
[3] J.J. Baschuk, X. Li, J. Power Sources 86 (2000) 181–196.
[4] T.E. Springer, T.A. Zawodzinski, S. Gottesfeld, J. Electrochem. Soc. 138 (1991) 2334–2341.
[5] M. Cappadonia, J.W. Erning, U. Stimming, J. Electroanal. Chem. 376 (1994) 189–193.
[6] M. Saito, K. Hayamizu, T. Okada, J. Phys. Chem. B 109 (2005) 3112–3119.
[7] H.A. Gasteiger, J.E. Panels, S.G. Yan, J. Power Sources 127 (2004) 162–171.
[8] U. Pasaogullari, C.Y. Wang, J. Electrochem. Soc. 151 (2004) A399–A406.
[9] A.Z. Weber, J. Newman, J. Electrochem. Soc. 151 (2004) A311–A325.
[10] Y. Hishinuma, T. Chikahisa, F. Kagami, T. Ogawa, JSME Int. J. Ser. B 47 (2004) 235–241.
[11] Y. Hishinuma, F. Kagami, personal communications, November 2005.
[12] R.K. Ahluwalia, X. Wang, A. Rousseau, J. Power Sources 152 (2005) 233–244.